

Simulation of flow around piers

Simulation d'écoulements autour de piles de ponts

KAMIL H. M. ALI, *Civil Engineering Department, University of Liverpool, U.K.*

OTHMAN KARIM, *Civil Engineering Department, University of Kebangsaan, Malaysia*

ABSTRACT

FLUENT CFD was used to predict the three-dimensional flow field around a circular cylinder. Solutions were obtained for rigid beds and for scour holes of different sizes resulting from different time-durations. The numerical results were used to obtain the variation of bed shear-stress around the cylinder. These results were used in the sediment continuity equation to obtain an expression for the variation of scour depth with time. The asymptotic scour depth was found to depend on three dimensionless numbers: the pile number, the sediment size number and the duration time number. The theoretical relationship was calibrated using various laboratory and field results.

RÉSUMÉ

Le code FLUENT CFD a été utilisé pour calculer l'écoulement tridimensionnel autour d'un cylindre circulaire. Les solutions ont été obtenues pour des lits rigides et pour différentes tailles d'affouillements résultant de durées différentes. Les résultats numériques ont permis d'obtenir la variation de la contrainte de cisaillement sur le fond du lit autour du cylindre. Ces résultats ont été utilisés dans l'équation de continuité du sédiment pour obtenir une expression de la variation en temps de la profondeur d'affouillement. On trouve que la profondeur limite d'affouillement dépend de trois nombres sans dimension relatifs à : la pile, la taille du sédiment, et la durée. La relation théorique a été étalonnée à l'aide de divers résultats obtenus en nature ou en laboratoire.

Introduction

The drowning of four rail passengers during the collapse of Glanrhyd Bridge on the swollen River Towy, October 1987, illustrated the dangers of scour. Lack of practical knowledge about scour has left some hydraulic experts claiming that the collapse of a large bridge caused by foundation erosion is a disaster waiting to happen. With over 150,000 road bridges and 6000 rail bridges in the U.K., the problem could pose a serious safety problem as well as significant financial burden (Penson, 1996). Although the provision of protection works is a common practice in the Netherlands and some other countries, this is not the case in the USA and the UK.

Continuous scour at a structure can lead to its failure, thus an understanding of the scouring process and the ability to predict the scour behaviour, is very important if steps in the design process are to be taken to protect against it.

Although the general flow field around a circular pier has been documented, the theoretical modelling of it has received little attention because the distribution patterns of the velocity components are complex. This paper gives applications of the computer package 'FLUENT' to simulate the complex flow field around piers. Several experimental set-ups used by previous researchers were chosen for model comparison. In addition to that, experiments were also conducted at the Hydraulic Laboratory, University of Liverpool, to assess the scour around grouped-piers arrangement under clear water regime.

Description of the Flow Patterns and Mechanism of Scour Around Piers

Piers for hydraulic structures such as bridges, barrages and regulators are often built in open channels. Generally, the structural engineer is concerned with the appearance of the piers in relation to the surrounding features, and the hydraulic engineer is concerned with the extent to which the piers cause obstruction to the flow, thereby affecting the flow pattern and dissipated energy. The scientific basis of structural design of bridges is highly advanced, but a unifying theory for estimating scour depth at piers is still in an embryonic stage, mainly due to the complex nature of the problem.

In recent years several papers have appeared dealing with aspects of scour at bridge piers. Most papers which are based on laboratory data, describe the behavioural pattern of bridge scour around cylindrical piers, avoiding the shape and alignment effects. This section reviews the general flow patterns and mechanism of scour around a cylindrical bridge pier as observed by previous researchers.

Piers, when introduced to a flow channel, result in significant changes to the flow pattern. A detailed description of the modified flow is essential to the understanding and analysis of the local scour which develops. The flow field around a pier is complex in detail, and the complexity is aggravated with the development of the scour hole. Detailed investigation on the flow pattern for such a case was reported by among others, Melville (1988), and Dargahi (1990). The important work on local scouring at piers was summarised by Breusers *et al.* (1977) and Dargahi (1982). Melville (1977) conducted a detailed study of the changing flow

Revision received August 14, 2000. Open for discussion till August 31, 2002.

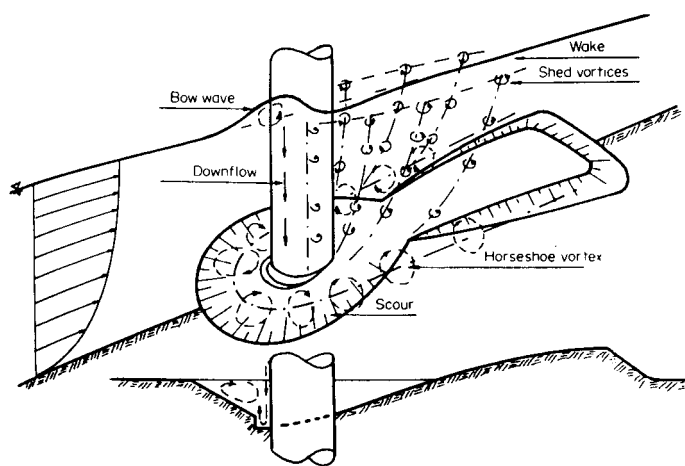


Fig. 1 Diagrammatic flow pattern at a cylindrical pier (after Raudkivi)

patterns at a cylindrical pier throughout the development of a local scour hole. The principal features of the flow pattern are shown in Figure 1. The flow decelerates as it approaches the cylinder coming to rest at the face of the pier. The associated stagnation pressures are highest near the surface, where the deceleration is greatest, and decrease downwards. In response to the downwards pressure gradient at the pier face, the flow reaches a maximum just below the bed level.

It is the downflow impinging on the bed which is the main scouring agent. The development of the scour hole around the pier also gives rise to a lee eddy, known as the horseshoe vortex. The horseshoe vortex is effective in transporting dislodged particles away past the pier and the two provide the dominant scour mechanism. Raudkivi (1986) noted that the horseshoe vortex is a consequence of scour, not the cause of it. The horseshoe vortex extends downstream, past sides of the pier, for a short distance before losing its identity and becoming part of the general turbulence.

The flow separates at the sides of the pier leading to the development of concentrated 'cast-off' vortices in the interface between the flow and the wake. These vortices are translated downstream by the mean flow and act like vacuum cleaners sucking up sediment from the bed.

Local scour occurs at a bridge site when the local flow field near the bridge piers is strong enough to remove bed materials. Local scour is a direct consequence of the flow obstruction caused by the bridge, the depth of scour being strongly dependent on the size of obstruction. Local scour is a time dependent process in which an equilibrium between the erosive capability of the flow and the resistance of motion of the bed material is progressively attained through erosion of the flow boundary. Scour hole development commences at the sides of the pier with the two holes rapidly propagating upstream around the perimeter of the cylinder to meet on the centreline. In this way, a shallow hole, concentric with the cylinder, is formed around most of the perimeter of the cylinder, but not in the wake region. The downflow acts like a vertical jet eroding a trench in front of the pier, the eroded material being transported downstream by the flow. During early stages of development of the scour hole the lip of the trench is often very sharp and the face is almost vertical. The trench be-

comes shallow or disappears completely when scour approaches the equilibrium depth. Excavation of the trench undermines the scour hole slope above, which collapses in local avalanches of bed material such that the slope angle is maintained. The collapsed material is ejected from the trench by the downflow and carried downstream by the flow where a bar develops. The upstream part of the scour hole has the shape of a frustrum of an inverted cone with slope equal to the repose angle of the bed material under erosion conditions.

Dargahi (1989) carried out an experiment to investigate by means of flow visualisation and measurements, the coupling between the flow field and local scouring. The general development of the scour pattern observed upstream of the pier along plane of symmetry with respect to time are illustrated in Figure 2.

Generally the equilibrium of final depth of local scour is rapidly attained in live-bed conditions, but rather more slowly in clear-water conditions, Figure 3. Observations of the equilibrium scour depth in live-bed conditions will show fluctuations in depth (the dotted line in Figure 3) due to the effects of feature migration.

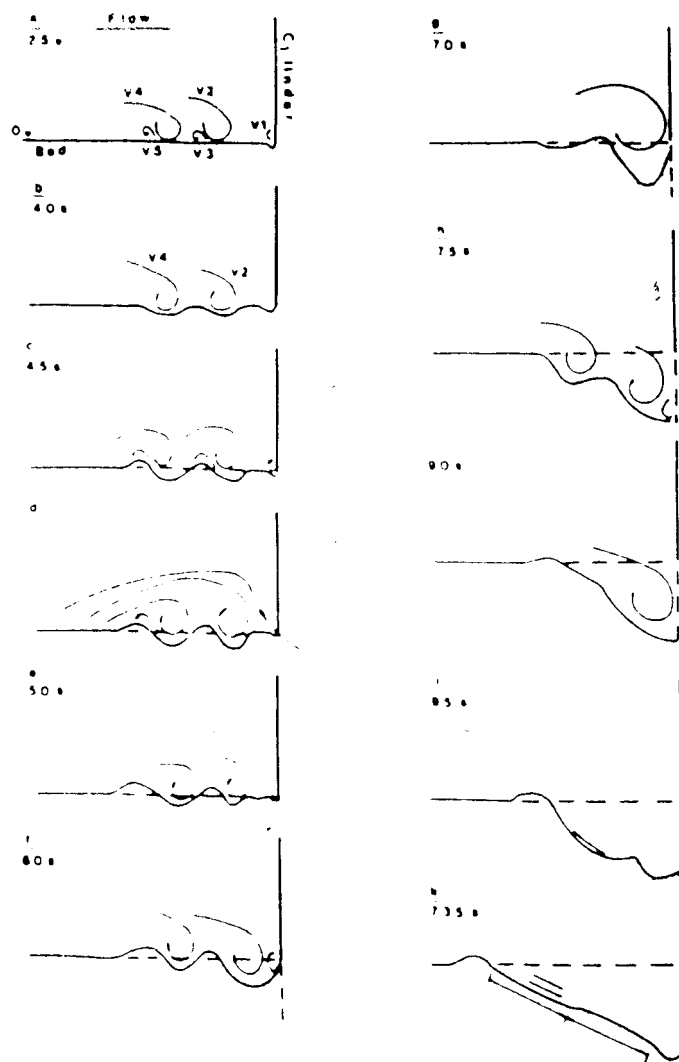


Fig. 2 General scour patterns upstream of cylinder along plane of symmetry (After Dargahi, 1989)

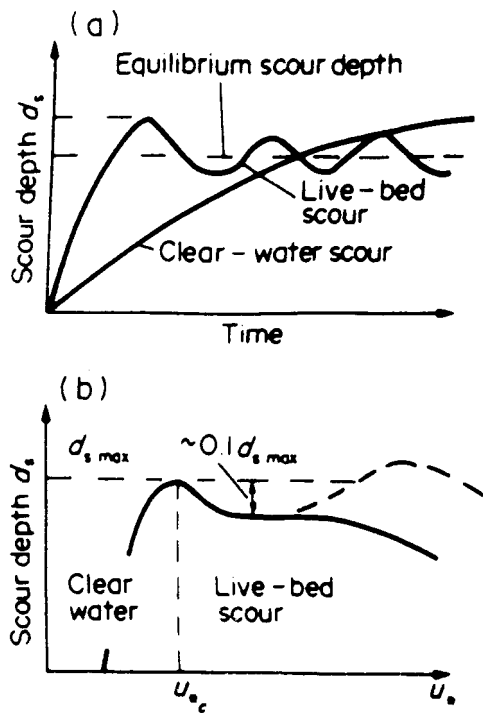


Fig. 3 Scour depth for a given pier and sediment size (a) as a function of time (b) as a function of shear velocity or approach velocity

Prediction of scour depth around bridge piers

Over the past 25 years numerous studies have been conducted and equations developed to predict bridge-pier scour. Most of these equations were developed using laboratory data and sometimes tested using limited field data. Due to the number of parameters influencing scour and the difficulty in quantifying them a number of different models have been developed each with different limitations. Raudkivi (1986) in discussing the functional trends of scour at bridge piers summarised the controlling factors for scour depth at bridge as: (a) Pier width or diameter; (b) type and gradation of sediment; (c) flow depth relative to pier width or diameter; (d) size of sediment relative to pier width; and (e) alignments of piers. The shape of piers according to him, has only a small effect and this can be easily overshadowed by random effects, such as rafts of floating debris or ice caught on the pier. He also concluded that the trends established in the laboratory may help researchers understand results from the field where interactions are frequently very complex and parameter values cannot be established.

An extensive comparison of seven of the more commonly used and cited pier-scour equations has been carried out by Johnson (1995). He compared the equations using a large set of field data, both live-bed and clear-water scour. Despite so many equations available to predict the scour depth, he concluded that there is still a need for additional research on the scour process, especially for the cases in which flow velocities are near the critical velocity and for wide piers in relatively shallow water.

Simulation using FLUENT

In this section, FLUENT applications to simulate flow pattern around piers are described. In order to examine the secondary flow in the present study, it is necessary to apply a fully three-dimensional circulation. The disadvantage with the three-dimensional approach is that it necessitates a more complex computer code and that the cost of calculations becomes greater. For a typical situation, a three dimensional calculation takes over an order of magnitude more computer resources than a two-dimensional approach. However, as mentioned above, if effects of secondary flow are important for a particular case, a three-dimensional approach is therefore necessary. The prediction of flow around piers is compared with experimental and numerical results wherever possible.

FLUENT simulations

For the present analysis, a three-dimensional grid system was generated for the FLUENT simulations. After several trial runs, the present grid arrangement was found satisfactory. A 45 x 28 non-uniform grid was mapped in the domain cross section (x-y plane). Figure 4 illustrates the grid that is generated. The grid was smoothed using the differential equation grid solver prior to being read into FLUENT. In FLUENT the grid was extruded into the z-direction with 20 grid lines in the vertical (z) direction. Such procedure may not be applicable in generating grid involving scoured bed, as will be discussed later, and usually requires the three-dimensional grid to be generated fully within PreBFC. The grid system consisted of half the flume and the cylinder, and a symmetry condition was applied on part of the wall. The inlet boundary and the exit boundary in the far wake were placed 3.0R and 6.0R (R being the radius of the pier) from the centre of the pier, respectively. A uniform velocity of 0.067 m/s was applied on the inlet boundary. The bed roughness factor, was calculated using a procedure given by FLUENT. Two different turbulence models were used; namely the k-M model, and the RNG k-M model.

Results and Discussions

Figures 5 (a) and (b) show the velocity vectors near the bed pre-

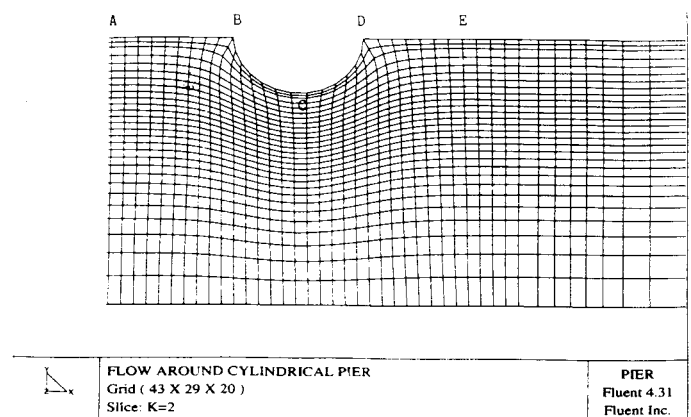


Fig. 4 Grid setup for Flow around Pier

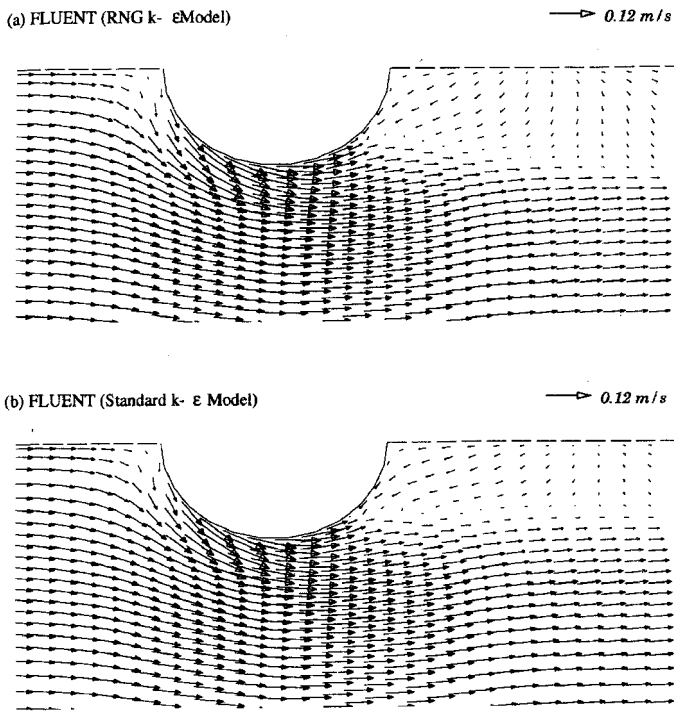


Fig. 5 Velocity Vectors near the bed

dicted by FLUENT using two turbulence models. Figures 6 (a) and (b) show the velocity vectors near the surface. The plots clearly show the existence of a separation zone behind the cylinder. The location of the separation point extend further downstream at the surface than close to the bed. Dey *et al.* (1995) observed in their study that the main characteristics feature of the flow around a pier on a flat surface are a relatively large secondary vortex flow field. The wake region in the numerical model results was defined as the region in which the longitudinal veloci-

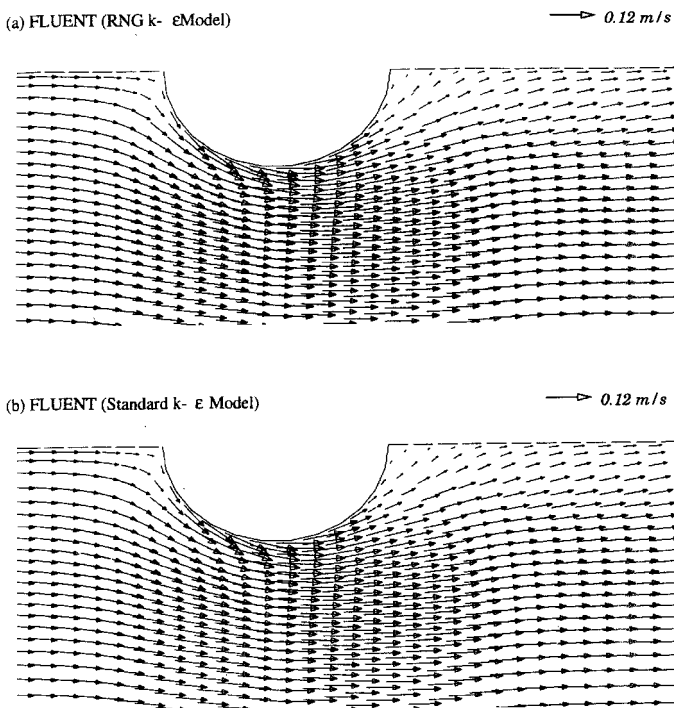


Fig. 6 Velocity Vectors near the surface

ties are in opposite direction to the main flow direction. This can be seen in Figure 5. The vorticity is an important quantity in a turbulence flow, since it is a measure for the intensity of the eddy motions, and the dynamics of turbulence are believed to be closely connected to vortex dynamics.

Comparison of the results from the two closure models adopted here show that the velocity fields are nearly identical.

A velocity map for the longitudinal profile along the symmetrical plane of the simulated domain is shown in Figure 7. The plot shows the existence of the horseshoe vortex downstream of the cylinder. This is in accordance with the flow description mentioned earlier.

Figure 8 (a) and (b) show the calculated bed shear stress distribution around the pier using two turbulence models. The shear stresses have been made non-dimensional by dividing the shear stress by the bed shear stress for the flume without the cylinder.

Experimental results of Yanmaz and Altinbilek (1990)

Yanmaz and Altinbilek (1990) conducted a series of experiments to study the development of scour around bridge pier models. The tests were carried out at the Hydromechanics Laboratory of Middle-East Technical University, Ankara, Turkey, using an L-shaped horizontal rectangular open-channel 90 cm deep, 67 cm wide with a concrete bottom. Side wall (except the test section for visual observations) are made of steel. Single bridge pier models made of plexiglass were set at the middle of the flume. Only clear water conditions with a flat bed were studied. No sediment inflow was allowed into the scour hole from upstream. Three different sizes of pier were used in the experiments, but for the present simulation purposes results for the pier with a diameter of 6.7 cm were selected.

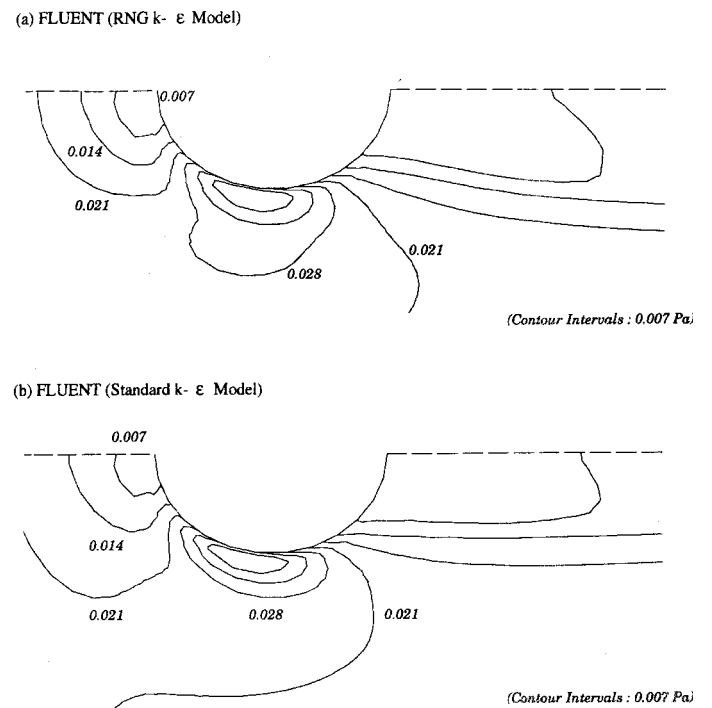
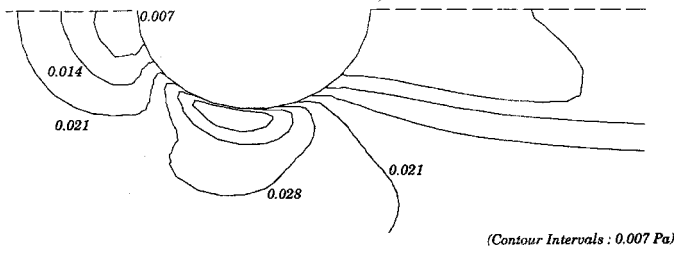


Fig. 7 Velocity Vector for longitudinal profile along centerline

(a) FLUENT (RNG k- ϵ Model)



(b) FLUENT (Standard k- ϵ Model)

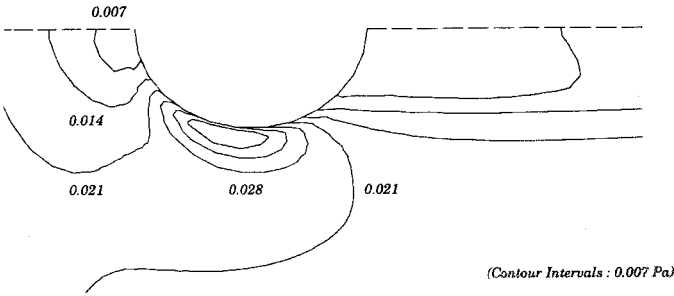


Fig. 8 Computed Bed Shear Stress Distributions

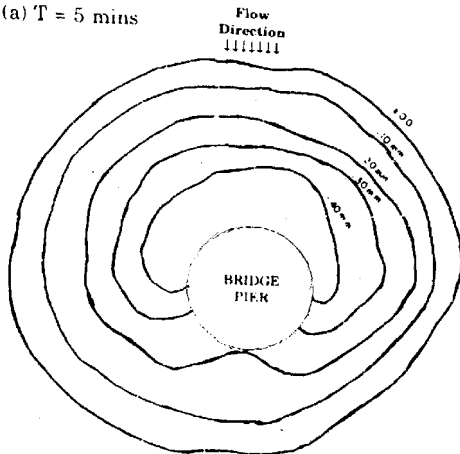
The materials used for the bed are quartz-sand with specific weights of 26.4 kN/m^3 , mean particle sizes of 1.07 mm with $[\rho_g = 1.13]$. Bed materials were placed as a 15 cm thick layer in the flume bed.

Experiments were stopped at the end of different time durations to determine the contours of the scour hole around the bridge pier. The bed topography for $T=5, 20, 60, 100$ and 150 mins are shown in Figures 9. Yanmaz and Altinbilek (1990) observed that the average side angle of the scour holes around the pier was approximately equal to 33° , which is close to the natural angle of repose of quartz sand.

FLUENT Simulations

Based on the bed contours provided by Yanmaz (1994), three-dimensional orthogonal grid systems of $60 \times 15 \times 12$ were generated for $T=0, 5, 60$ and 150 mins. Typical grid distribution is shown in Figure 10. The grid lines are packed together at an area surrounding the pier. As the bed contours are almost symmetrical along the axis of the cylinder parallel to the flow direction, only half of the cylinder were modelled, and a symmetry condition was applied on part of the wall. A uniform velocity of 0.33 m/s

(a) $T = 5$ mins



(b) $T = 60$ mins

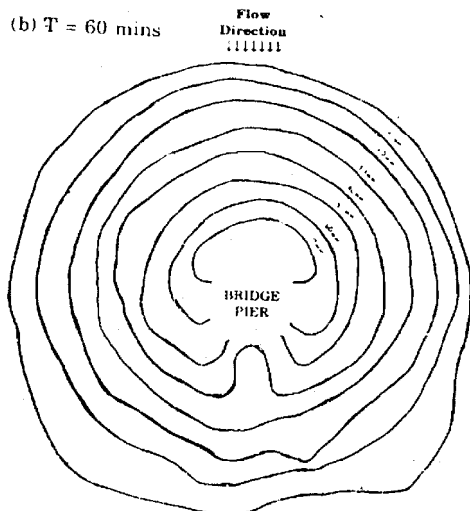
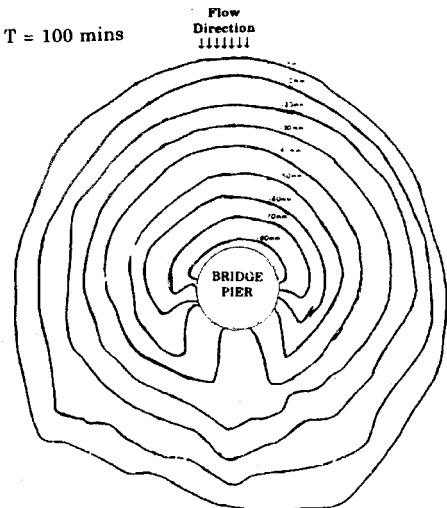


Fig. 9a Topographic map around Pier (a) $T = 5$ mins; (b) $T = 60$ mins (after Yanmaz, 1994)

(c) $T = 100$ mins



(d) $T = 150$ mins

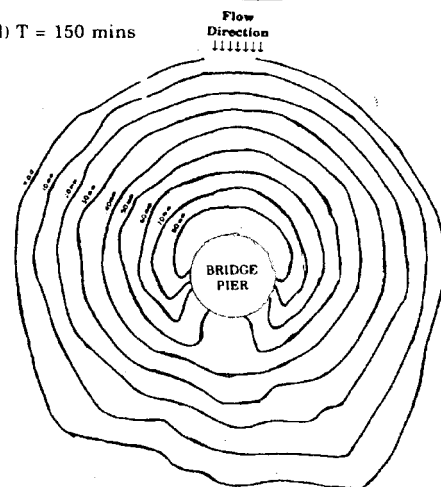


Fig. 9b Topographic map around Pier (c) $T = 100$ mins; (d) $T = 150$ mins (after Yanmaz, 1994)

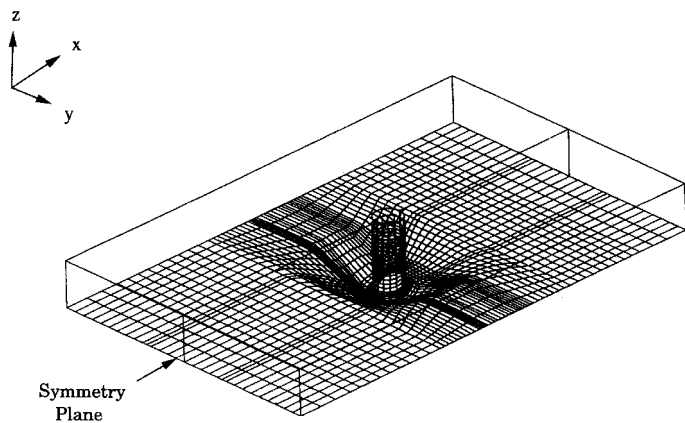


Fig. 10 Typical Grid setup (k=1) for FLUENT simulation (T = 150 mins)

was applied at inlet boundary, located 12R (R being the diameter of the pier) upstream of the centre of the pier. Similarly the outlet was located 12R downstream. It is important to note here that FLUENT V4.3 cannot simulate a free surface directly. The water surface was modelled by means of a 'rigid-lid' boundary. The surface is approximated as a frictionless wall or slip wall, that is links to all scalar components were cut. Such assumption, therefore, will not allow FLUENT to simulate any changes in water level.

Results and Discussions

Figures 11 - 14 show the predicted velocity vectors and bed shear stresses for T=0, 5, 60 and 150 mins, respectively. FLUENT reported the bed shear stress in term of X, Y and Z components. As the flow reaches the pier, separation occurs and the Y-velocity component becomes significant. This can be seen from the figures where the Y-component bed shear stresses are relatively high compared to the X-component bed shear stresses. The negative sign indicates the direction of the flow with respect to the sign convention used.

Fluent's shear stress results depend on the absolute size of the cells within the solution grid. This is an important issue since if the cells are too large, the solution obtained can be dependent on the cell size rather than purely on the physical constraints of the solution domain and the input conditions. It is therefore desirable to keep cell sizes small in order to avoid a grid-dependent solution. Output given by FLUENT corresponds to values stored at the centre of each grid cell. Karim (1996) conducted a systematic investigation of the effect of grid size on boundary shear stress values and optimum values were used in this study. Using modified Shields Diagram (Vanoni, 1975, p.99), the flat-bed critical shear stress, τ_c , for the material used in the experiment was calculated to be 0.48 N/m^2 . It can be seen from Figure 11 that at some locations, especially at the neighbouring area of the pier, the predicted bed shear stress values exceeded the critical shear stress for the particles and therefore transport may be expected. It is interesting to note that Raudkivi (1986) in his paper stated that local scour in such case is due to the interference with the flow by the piers. He further stated that local scour at a pier commences when the shear velocity, u_* , or velocity U exceeds about half the critical

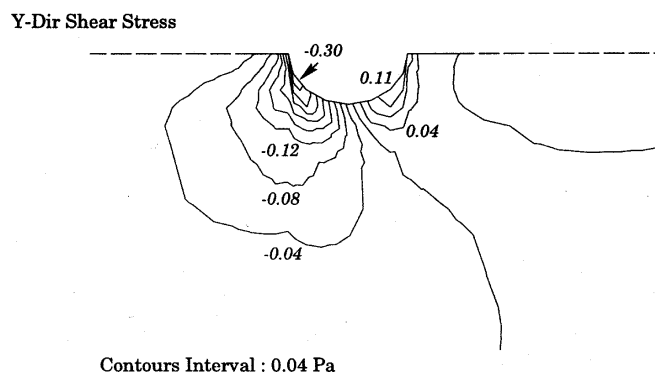
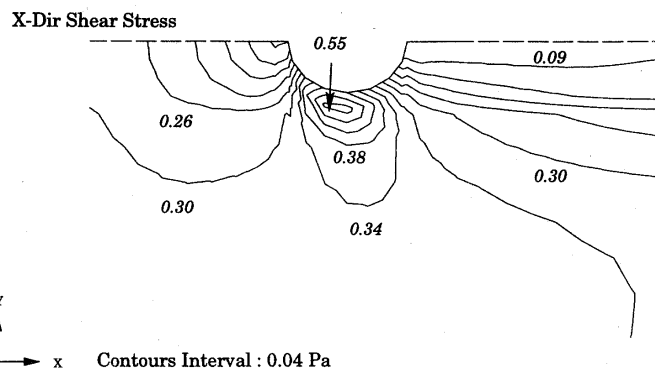
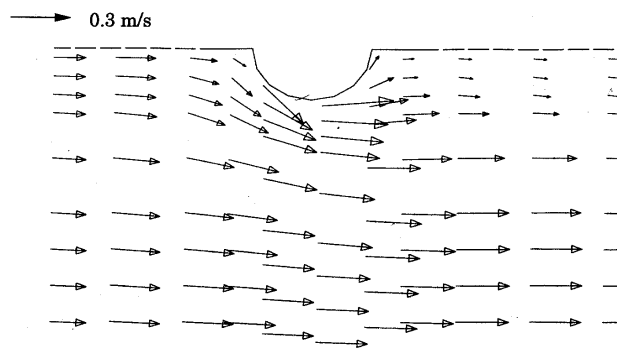


Fig. 11 Bed velocity vectors and shear-stress contours (Initial flat-bed)

threshold value for movement of the sediment. While the scour depressions at the sides of the cylinder deepen, the side slopes develop into the scour hole and sediment becomes very unstable (Dargahi, 1990). The instability causes sliding of sediment on the upper slope and this further increase the rate of transport. Since both drag (or shear) and self weight components are combining to dislodge the sediment, the shear required to move the grain downslope must essentially be less than the critical bed shear stress for the flat-bed. Lim (1985) in his study employed a formula derived by Brooks (1962) to determine the critical shear stress correction for bed slope. The formula is given as:

$$\frac{\tau_{sc}}{\tau_c} = -A \pm \sqrt{A^2 + B} \quad (1)$$

where τ_c = critical shear stress on a flat bed
 τ_{sc} = corrected critical shear stress using Brook's formula

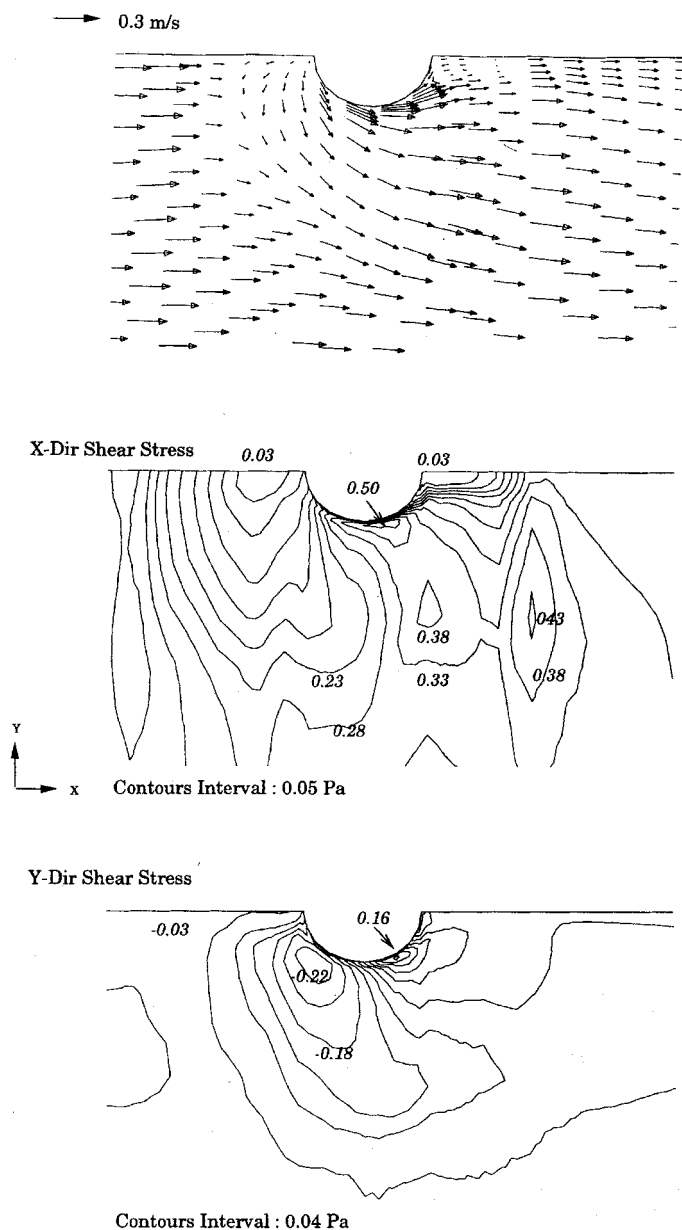


Fig. 12 Bed velocity vectors and shear-stress contours (T = 5 mins)

- A = $(\sin\phi \sin_) / \tan\theta$
- B = $1 - (\sin^2\phi / \sin^2\theta)$
- ϕ = slope angle of bed profile (+ve downward slope)
- $_$ = angle between flow direction and slope direction measured in the plane of the slope
- θ = static angle of repose of sediment ($=33^\circ$)

To illustrate, consider downward slope along the symmetrical plane upstream of the pier for T=60. From Figure 9 the downward slope is calculated to be 29.7° . Taking $\alpha = 0$, as the direction of the velocity vector is parallel to the bed profile, the modification factor for critical bed slope using the above equations is equal to 0.42. This indicates that the critical bed shear stress for sloping bed reduces to almost half of the critical shear stress for the flat bed. For T=5 and 150 mins, the upstream downward slope is equal to 35.6° and 33° , respectively. The slope at T=5 mins exceeded the natural repose angle of the sediment. At this stage, the slope is caused mainly by the vortices and the reverse flow re-

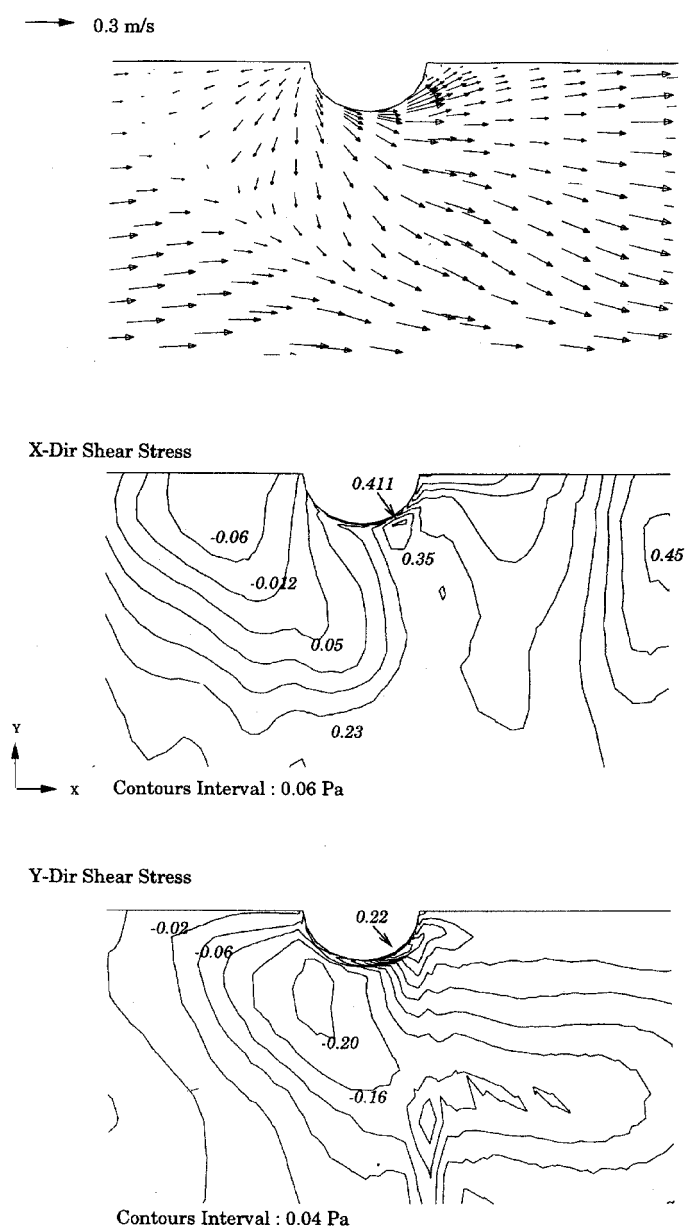
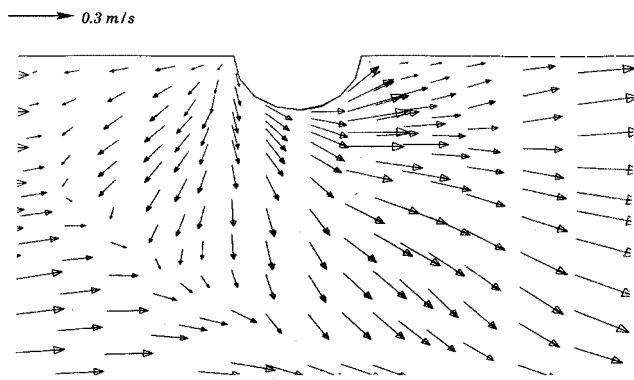
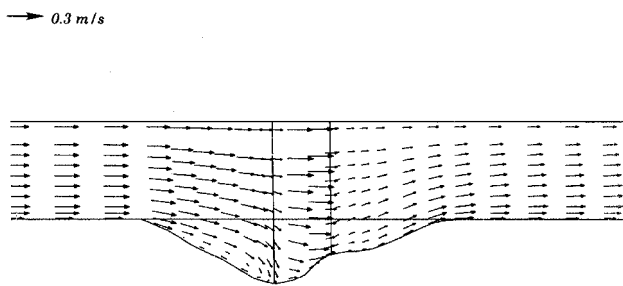


Fig. 13 Bed velocity vectors and shear-stress contours (T = 60 mins)

flected by the pier, analogous to the processes shown in Figures 2. As the hole becomes deeper, the sediment on the upper slope continue sliding until all the forces acting on the bed reach equilibrium. At this stage the slope of the bed is equal to the repose angle of the sediment (i.e. 33° at T=150 mins). Figure 14 b shows the longitudinal velocity vectors along the symmetrical plane. The plot indicated the presence of a downward flow at the face of the pier. In addition to the shear forces acting on the bed, it can be inferred that the downflow may also exert forces on the bed that initiate the eddy which causes the increase of local scour around the pier. Figure 15 shows the downflow velocity plot in front of the pier for T=0, 5, 60 and 150 mins. It can be concluded from this plot that the vertical downward flow in front of the pier increases with the increase in scour hole depth, until an almost equilibrium stage is reached. From Table 1 it can be seen that the maximum bed shear stress decreases as the hole becomes deeper. The shear stress value at the brim of the scour hole (flat bed) along the symmetrical plane



(a) near bed



(b) longitudinal profile along centerline

Fig. 14a Velocity vectors (T = 150 mins)

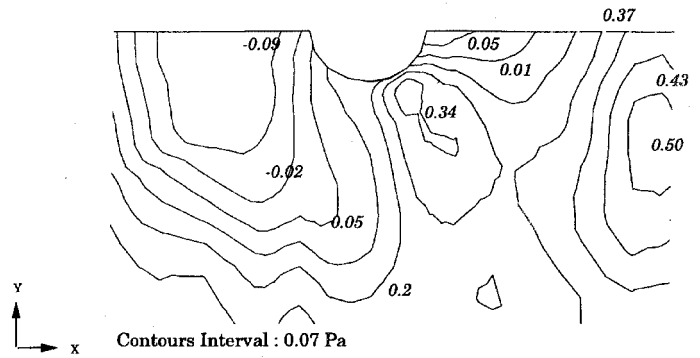
for each case is essentially less than the critical flat-bed shear stress, marking the boundary of the scour hole.

Table 1 Maximum Shear Stress Around Pier

Time (mins)	Calculated Max. Shear Stress (Pa)		Shear Stress at the brim of scour hole (upstream of pier) along symmetrical plane (Pa)
	X-Direction	Y-Direction	
0	0.55	0.30	-
5	0.50	0.22	0.288
60	0.41	0.22	0.265
150	0.34	0.20	0.236

In the downstream region of the hole (Figure 14 b), the decrease in depth between the bed and the 'fixed' water surface causes the flow to converge. According to principle of continuity, the velocity at this section will increase, so does the bed shear stress. In practise this might not be so, as this upward flow may be translated as an increase in water level. Thus, the velocity will not be as high as predicted by the numerical model. As mentioned be-

X-Dir Shear Stress



Y-Dir Shear Stress

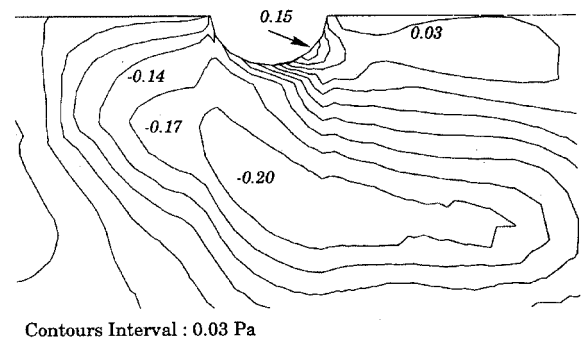


Fig. 14b Bed shear-stress contours (T = 150 mins)

fore, FLUENT is not able to simulate the increase in the water surface. A simplification is used by assuming the free surface to be represented by a smooth 'closed-lid'. On that note, the results reported by FLUENT in such cases must be judged with great care.

Experimental work at Liverpool

Experiments were conducted in a glass-walled wave-current flume at the Hydraulics Laboratory of the University of Liverpool to study the development of scour holes around piers. Bed contours were provided by Yanmaz (1994) (Figure 9). These were used to form plaster moulds of the scour holes which were then coated with sand of a median size of about 1mm. Each plaster cast was placed in the flume together with a circular pile 67mm in diameter. The flume contained a sand bed of the same size. Steady state experiments were conducted for a water depth of 155mm and an average upstream velocity of 0.3m/s. Detailed velocities were measured along the X and Y direction 8mm above the bed. These were obtained using a Nixon propeller meter 16mm in diameter. Shear stresses 'near the bed' were calculated from $\tau_0 = (\rho f U_b^2) / 8$ where f = friction factor and U_b = velocity near the floor.

Figure 16 shows experimental 'near the bed' shear stress distributions for T = 0, 5, 20 and 100 minutes. As expected, there is a general reduction in shear stresses with time, i.e. as the scour hold becomes bigger. Using these results, shear values along the line ABCDE (Figure 5) were obtained and are shown in Figure 17 together with the corresponding values from FLUENT. Clearly,

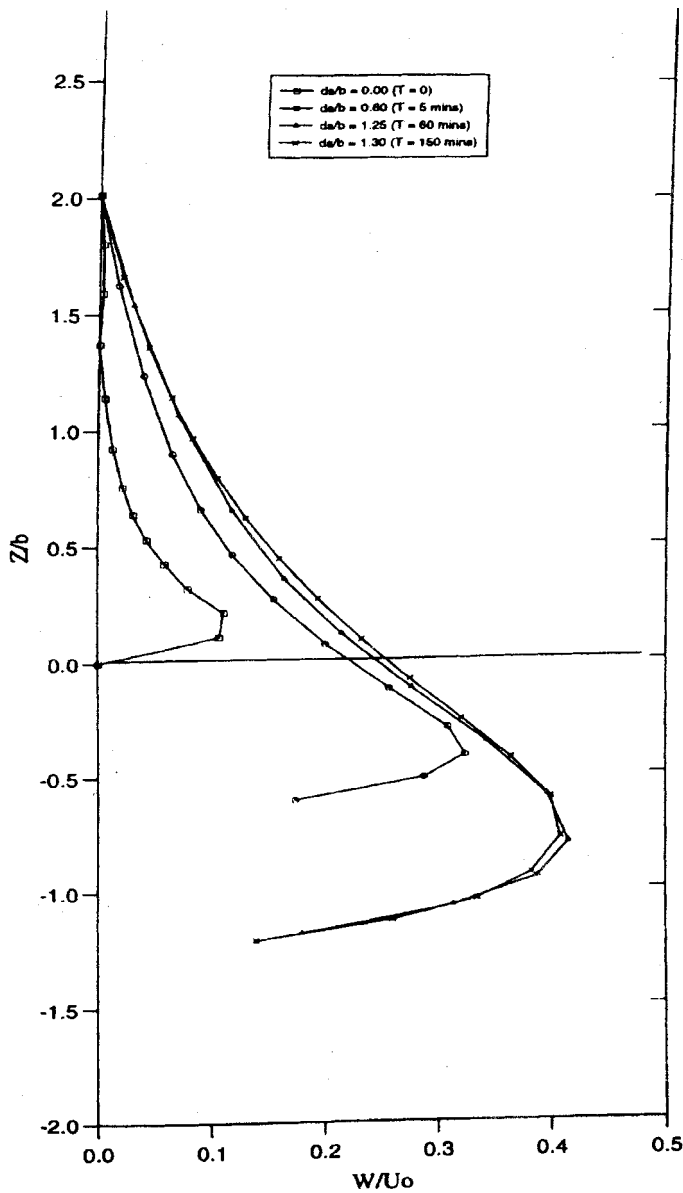


Fig. 15 Downflow velocity W in front of pier (U_0 = uniform inlet velocity, Z = height above initial bed level, b = diameter of pier)

changes are much more marked in the FLUENT results which are generally higher than the experimental ones. This is to be expected as the experimental shear stresses are measured 8mm above the bed. Also, it is unlikely that FLUENT can reproduce accurately the very complicated system of vortices and the work associated with this problem.

Prediction of maximum scour depth profile

Observations of experimental results show that maximum scour takes place along the line A B C D E (Figure 5). Figure 18 shows scour hole profiles along this line for different values of T . These results were obtained from Figure 9. Using these results, dimensionless profiles were obtained and are presented in Figures 19 and 20. Clearly, the Gaussian distribution gives a better agreement with the experimental results than does the cosine profile. Figure 30 shows that the scour hole profiles, when plotted in this form, are similar. This means that the bed profiles, for different

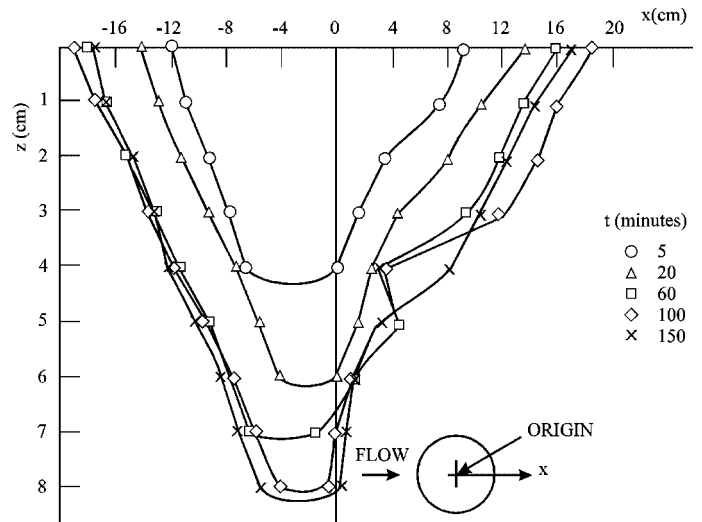


Fig. 16 Maximum scour holes profiles for a single pile

time periods, can all be expressed by one relationship. Variations of Z_{max} and x_m with time are then required. This approach usually results in considerable simplification of the analysis as is the case, for example, of turbulent free jets.

The theoretical values of total boundary shear stress along line A B C D E obtained using FLUENT were used to calculate the sediment discharges along this line using the relationship given by Van Rijn (1984) for sediment discharge.

Variation of τ_0 with x/D along the line ABCDE is shown in Figure 21 using Yanmaz et al's (1994) experimental bed contours. These experiments were for $U_0 = 33$ cm/s, $h = 15.5$ cm and $d = 1.07$ mm and for time periods of 5, 60, 100 and 150 minutes (see Figure 9). Also given are the curves for $T = 0$ and interpolated curves for $T = 10, 20, 30, 40, 50,$ and 140 minutes.

Van Rijn's (1984) relationship for sediment discharge is:

$$q_s = 0.1 [(S-1)g]^{1/2} d^{3/2} D_*^{-0.3} T^{3/2} \quad (2)$$

where

S = specific gravity of particle; g = acceleration due to gravity; D_* dimensionless particle diameter given by

$$D_* = \left[\frac{(S-1)g}{v^2} \right]^{1/3} \quad (3)$$

and T = dimensionless bed-shear parameter given by

$$T = (\tau_0 - \tau_c) / \tau_c \quad (4)$$

where

τ_0 = boundary shear stress and τ_c = critical shear stress.

The one-dimensional sediment continuity equation along line A B C D E (Figure 5) is approximately given by:

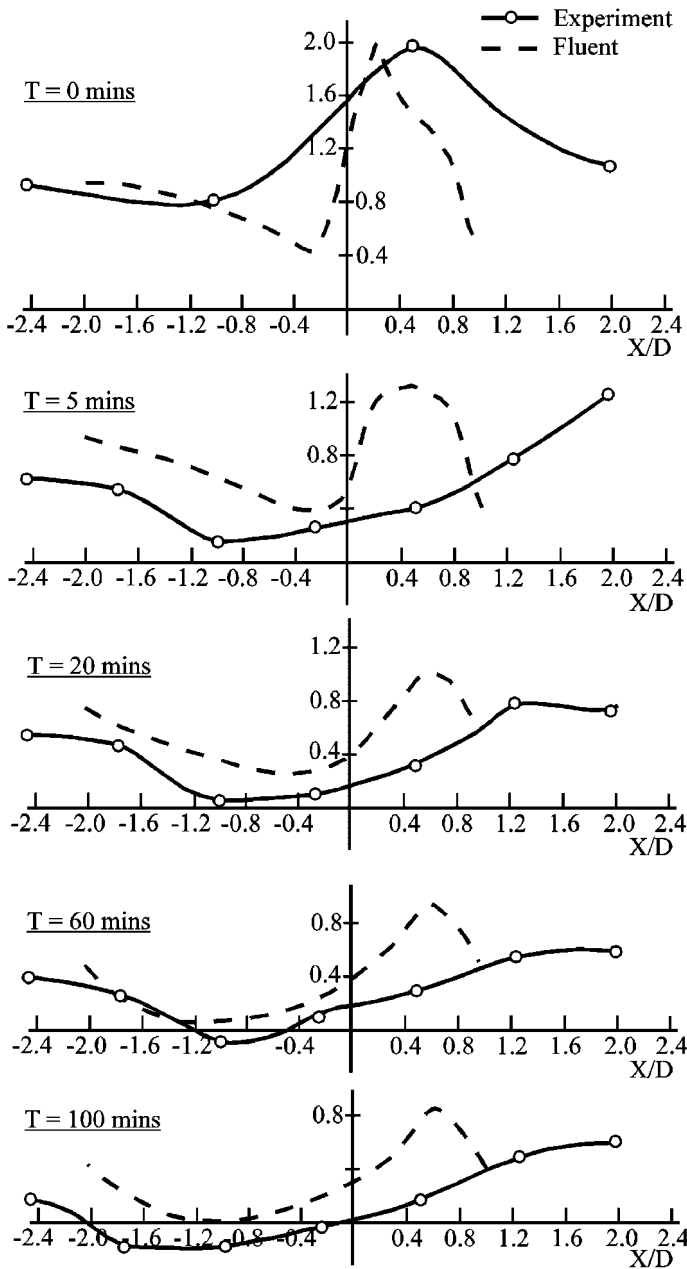


Fig. 17 Comparison between experimental and theoretical boundary shear stresses

$$(1-p)\frac{\partial z}{\partial T} + \frac{\partial q_s}{\partial x} = 0 \quad (5)$$

where p = porosity; z = elevation of the bed above a datum; T = time from beginning of the scouring process and x = developed length along ABCDE with its origin at B and being positive in the flow direction.

Using Figure 21, the variation of $T^{3/2}$ with x/D was obtained and is shown in Figure 22. It must be stressed that the critical shear stress τ_c is a function of x . It was assumed that the values of τ_0 , for various x , at $T = 150$ minutes represented the threshold conditions, i.e. when $T = 150$ minutes $\tau_0 = \tau_c$.

The variation of $T^{3/2}$ with x/D , shown in Figure 20, can be well represented by

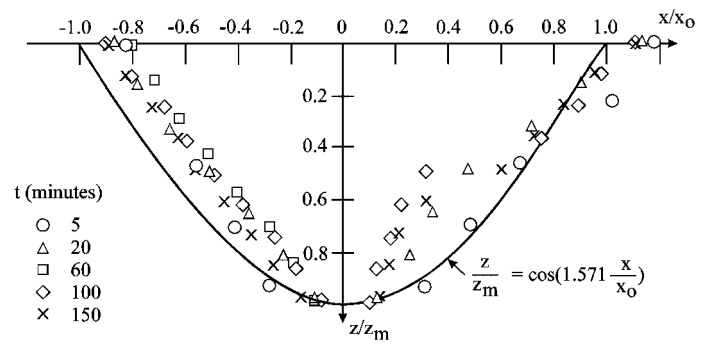


Fig. 18 Dimensionless scour hole profiles around a circular pile

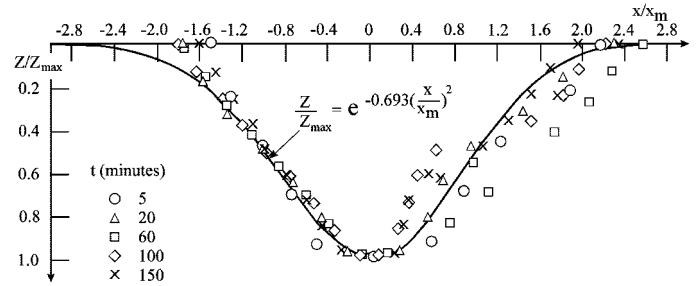


Fig. 19 Dimensionless maximum scour hole profiles

$$T^{3/2} = T_{\max}^{3/2} \text{Exp} \left[-30.81 \left(\frac{x}{D} + 1 \right)^2 \right] \quad (6)$$

$$T_{\max}^{3/2} = T_{\max 0}^{3/2} \text{Exp} \left[-5.32 \times 10^{-4} \frac{U_0 T}{h} \right] \quad (7)$$

where $T_{\max 0}^{3/2}$ = value of $T_{\max}^{3/2}$ at $T = 0$

Substituting from Eqs. (6) and (7) into Eq. (2), we obtain

$$q_s = K_1 T_{\max 0}^{3/2} \text{Exp} \left[-5.32 \times 10^{-4} \frac{U_0 T}{h} \right] \text{Exp} \left[-30.81 \left(\frac{x}{D} + 1 \right)^2 \right] \quad (8)$$

where

$$K_1 = 0.1 [(S-1)g]^{1/2} d^{3/2} D_s^{-0.3} \quad (9)$$

Differentiating Eq. (8), substituting in Eq. (5) and integrating, we get

$$z = \frac{a_0 K_1 h}{U_0 D} T_{\max 0}^{3/2} \left(1 + \frac{x}{D} \right) \text{Exp} \left[-a_2 \left(1 + \frac{x}{D} \right)^2 \right] \left[1 - \text{Exp} \left(-a_1 \frac{U_0 T}{h} \right) \right] \quad (10)$$

where

$$a_0 = 1.158 \times 10^5, a_1 = 5.32 \times 10^{-4} \text{ and } a_2 = 30.81$$

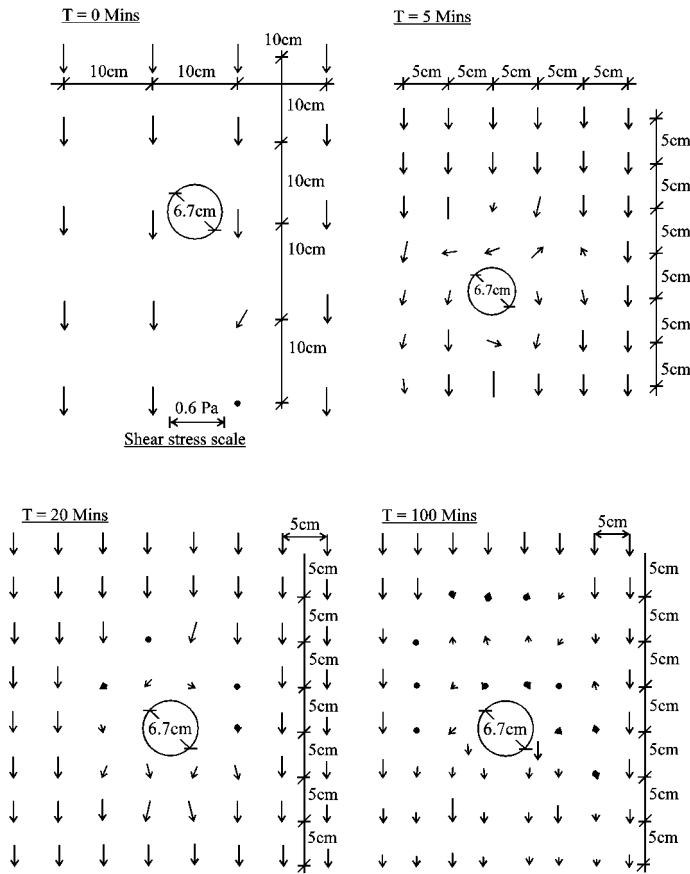


Fig. 20 Experimental bed shear stress distributions

We obtain the maximum value of z , for a given T , by putting $\partial z/\partial x = 0$ in Eq.(10). This gives $x/D = -0.873$ and

$$\frac{z_{\max}}{h} = \frac{K}{R} \left[1 - \text{Exp} \left(-a_1 \frac{U_0 T}{h} \right) \right] \quad (11)$$

where $R = U_0 D/\nu$ and $K = K_1 D_*^{1.2}$ (12)

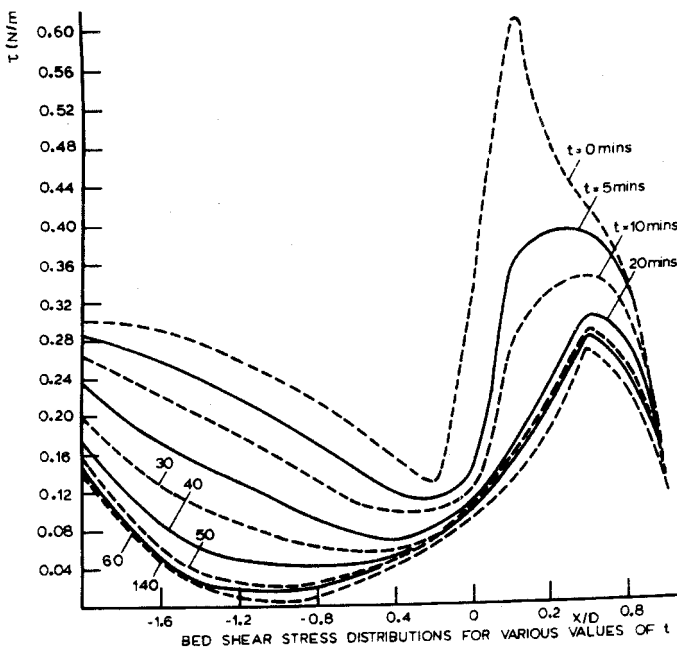


Fig. 21 Bed shear stress distributions for various values of t

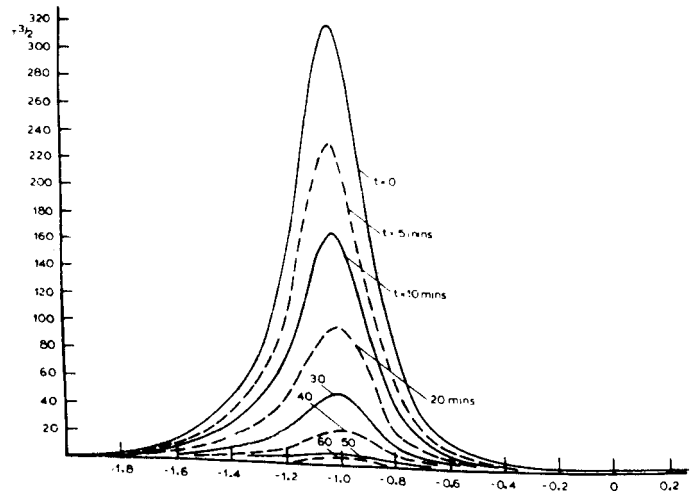


Fig. 22 Variation of $T_{3/2}$ with X/D

Equation (11) was verified using laboratory and field results:

Verification of the Theoretical Relationship For Maximum Depth of Scour Hole

Various model and field measurements of the scour around bridge piers were used to verify Eq. (11):

1. Laboratory Experiments

(i) *Yamaz and Altinbilek (1991)*

They conducted extensive experiments using circular and square piles. Diameters of the circular piles were 6.7, 5.7 and 4.7 cm. Sand particles with median size of 1.07 and 0.84 mm were used. All of the experiments were carried out for clear water scour. Values of K in Eq. (12) were calculated for the circular piles and are plotted as a function of the piles Reynolds number in Figure 23.

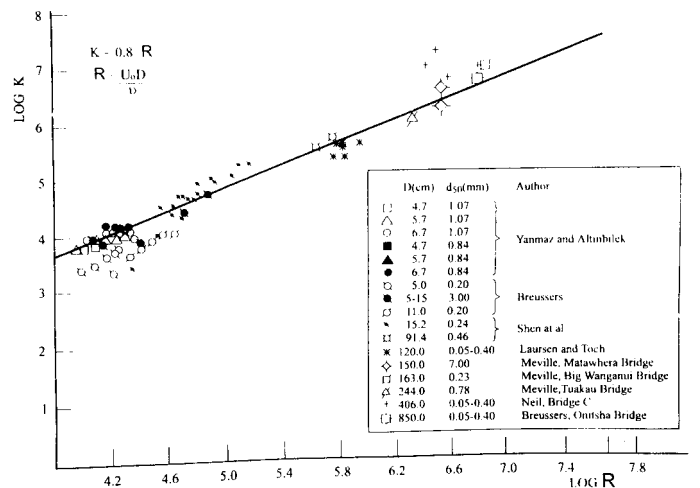


Fig. 23 Variation of $\log K$ with $\log R$ for various model and prototype bridges

(ii) *Shen et al (1969)*

Experiments were conducted using a 15.2 cm diameter circular pile using sand with $d = 0.24$ mm. Two additional experiments were carried out using $d = 0.46$ mm.

Two experiments were also performed using a pile 91.4 cm diameter and particles with $d = 0.46$ mm.

Calculations show that almost all of Shen et al's experimental results are for live bed scour.

(iii) *Breusers H. N. C. (1971)*

He carried out experiments using piles with $D = 5$ and 11 cm, water depths of 15 , 25 , and 50 cm. Sand particles with $d = 2$ mm were used. Experiments were carried out for fixed values of U_0/U_{0c} (U_{0c} = critical water velocity for the initiation of bed movement).

2. Field Measurements

(i) *Laursen and Toch (1956), Skunk River*

Prototype measurements were carried out at the nose of a single rounded pier in the middle of a straight reach of a sand-bed river. The width of the pier was approximately 1.2 m. The maximum scour depth was 2.0 m at a flow depth of 3.7 m. No mention is made regarding the mean velocity of flow or the median size of the sand particles.

Following the results of Alam and Kennedy (1969), the present authors assumed that d covered the range $0.05 - 0.40$ mm. Lacey's Regime Theory Raudkivi (1990) was used to calculate the mean velocity of flow. Values of K were calculated using Eqs 11 and 12.

(ii) *Neil, C. R. (1964)*

He reported several cases of scour near bridges which in some cases led to bridge failure. In the case of Bridge C, slender piers were supported by a concrete caisson from 10.6 m below the bed to 1.5 m above it. The bed was composed of sand and the pier was skewed at least 40° to the current. The median particle size was not given and was assumed to cover the range $0.05 - 0.40$ mm.

(iii) *Breusers (1971), Onitsha Bridge, Niger River*

The piers consisted of two circular piles having diameters of 8.5 m and a centre-line separation of 17 m. The mean depth of flow of 9 m and the mean velocity was 0.7 m/s. The actual scour depth was 7.6 m. Raudkivi's Figure 9.16 was used to obtain the scour depth for a single pile (= 6.8 m). The value of K was obtained assuming that $d = 0.05 - 0.40$ mm.

(iv) *Melville (1975), Big Wanganui River Bridge*

We have $U_0 = 4.27$ m/s, $h = 3.8$ m and $d = 0.23$ mm. The pier

measured 8.50 m x 1.63 m and the angle of attack of the flow was 10° . The estimated scour depth was 4.90 m.

The maximum depth of scour hole for an equivalent cylindrical pier was obtained using Figures provided by Breusers (1977) to account for the actual shape of the pier and for the angle of attack of the flow.

(v) *Melville, (1975), Matawhera Railway Bridge*

In this case the pier diameter was 1.5 m and the median particle size was 7 mm. The water depth was 3.0 m and the mean velocity was 2.25 m/s.

(vi) *Melville (1975), Tuakau Bridge, Lower Waikato River*

The mean water depth was 3.0 m, the mean velocity was 0.87 m/s and the median particle size was 0.78 mm. The pier shape was rectangular with dimensions 8.85 by 2.44 m with chamfered corners and an angle of attack of 10° .

Despite of all the limitation, in general, FLUENT exhibits good qualitative predicted flow patterns around the piers. Further detailed and rigorous study need to be carried out to validate the results quantitatively. The ability of rapidly growing CFD package to model a complex flow such as described in this paper would provide a powerful tool in manipulating tests and analytical approached complementarily in order to predict the scour depth under various conditions and furthermore to devise effective disaster prevention work against local scouring.

Using the shear stress distributions provided by FLUENT, an expression was derived for the time variation of the scour depth. The maximum depth of scour was shown to be a function of D_* , R , and $U_0 t/h$.

An attempt was made to verify the authors' relationship using various model and field data. Unfortunately, most of the field results were of poor quality, often lacking in important details. Approximately, it was found that the maximum depth of scour was proportional to the water depth:

$$\frac{z_{\max}}{h} = 0.8 \left[1 - \text{Exp} \left(-a_1 \frac{U_0 T}{h} \right) \right] \quad (13)$$

$$\text{OR } \underline{z_{\max}} \propto h \text{ for large } a_1 U_0 T/h$$

Yanmaz and Altinbilek (1991) produced a diagram (their Figure 1) giving the variation of Z_{\max}/D against h/D using the laboratory results of many researchers. These results are given for cylindrical piers and cover a wide range of flow Froude numbers under live bed and clear water conditions. Figure 24 shows a comparison between the results of eight of the researchers and Eq. (13) for large T . Except for Basaketal's results, there is reasonable agreement. It must be stressed that Eq. (13) was derived for clear water scour. Also, the parameter K , in Eq. (11), was calibrated using laboratory and field results.

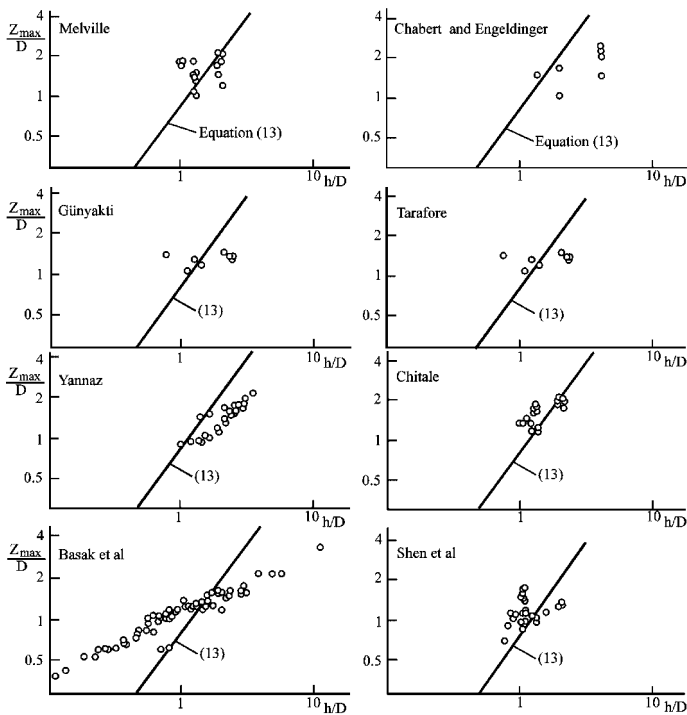


Fig. 24 Verification of equation 13 for large time periods

Conclusions

The collated three-dimensional turbulence formulation in FLUENT has been validated against selected benchmark solution of flow around piers. The flow field predicted by FLUENT seems to correspond quantitatively well with limited available experimental results. However, there was only a fair agreement between the bed shear stresses predicted by FLUENT and those calculated from the experimental velocities 'near the bed'. Much more refined measurements are needed for proper verification of FLUENT's results. The theoretical aspects of the flow dynamics, such as the horseshoe vortex, can also be interpreted from the output. The results obtained using the RNG $k-\epsilon$ model are virtually identical to those produced by the $k-\epsilon$ model.

After the scouring action had started, the bed shear stress fell and as the scour hole developed further the reduction became less apparent. The overall bed shear stress decreased with the increase in scouring time and with the increase in size of local scour. In general, the FLUENT results show that regions with the highest values of bed shear stress correspond to the region of highest floor velocity. The shear stress, predicted by FLUENT, is lowest in the region of maximum erosion and is highest near the rim region. At maximum erosion the cross sections of flow increased and from the continuity equation the mean velocity of the flow is expected to reduce. Similarly at the crest the area decreases and causes an increase of flow velocity. In practise the change in the bed level may result in fluctuation of the water level. FLUENT, however, is not capable of taking this in effect as it modelled the water surface as 'close-lid'.

It can be concluded that the boundary shear stress alone did not account for the entrainment and transport of the sediment particles. The degree of the turbulence intensity, especially in an obstructed flow field also contributed significantly in the scouring

process. In a physical model, not all relevant quantities could be furnished. Some physical quantities in a turbulence flow are difficult to measure. One of these quantities is the vorticity, which was known to be the major factor responsible for base scouring. With recent advances in flow visualisation technique, the measurement of this quantity is coming into reach of the experimentalist. In the present experiments, however, a very crude technique was employed. This did not provide adequate information for direct comparison with the results obtained from the numerical study.

On the other hand, it should also be expected that 'perfect' results are difficult to obtain in view of the many factors involved which cannot be modelled directly using a numerical simulation. For instance, the presence of 'turbulent bursts' which are widely observed and are capable of removing sediment from the bed. This results in enlargement of the scour hole. Unfortunately, FLUENT is not capable of predicting these bursts.

References

- ALAM, A.M.Z. and KENNEDY, J.F. (1969). 'Friction factors for flow in sand-bed channels', *J. of Hyd. Div. ASCE*, Vol. 95, No. HY6, Nov., pp 1973-1992.
- BREUSERS, H.N.C., '1971', 'Local scour near offshore structures', Proc. Symp. on Offshore Hydrodynamics, Wageningen.
- BREUSERS, H.N.C., NICOLLET, G., SHIEN, H.W. (1977). 'Local Scour Around Cylindrical Piers', *J. Hydr Res.*, ASCE, 15(3), 1977 pp 211-252.
- BROOKS, N.H. (1962), discussion of 'Boundary Shear Stress in Curved Trapezoidal Channel' by A.T. Ippen and P.A. Drinker. (Proc. Paper 3273) *J. Hydr. Div ASCE*, Vol 88. HY3, May 1963, pp. 327-333.
- BUTTERWORTH, G. (1996). 'Investigation of Local Scour Caused by Currents and Waves', *B.Eng. Thesis*, University of Liverpool.
- DARGAHI, B. (1990). 'Controlling Mechanism of Local Scouring', *J. Hydr. Engrg*, ASCE,, Vol 116, No.10, pp. 1197-1214.
- DARGAHI, B. (1982). 'The Turbulent Flow Field Around a Circular Cylinder', *Experiments in Fluids*, 8, pp. 1-12.
- JOHNSON, P.A. (1995). 'Comparison of Pier-Scour Equations Using Field Data', *J. Hydr. Engrg.*, ASCE, Vol 121, No. 8, pp . 626-629.
- KARIM, O. A., (1996). 'Prediction of Two and Three Dimensional Turbulent Flows', PhD Thesis, University of Liverpool, U.K.
- LAURSEN, E.M., TOCH, A., 1956, 'Scour bridge piers and abutments', Bull. No. 4, Iowa Highway Res. Board.
- LIM, S.Y., (1985) 'Scour and particle diffusion caused by water jets' PhD Thesis, University of Liverpool, UK.
- MELVILLE, B.W., 1975, 'Local scour of bridge sites, Univ. of Auckland, School of Engineering, Auckland, New Zealand, Report No. 117.
- MELVILLE, B.W. and RAUDKIVI, A.J., (1977). 'Flow characteristics in Local Scour at Bridge Piers', *J. Hydr. Research*, ASCE, Vol 15, pp. 373-380.
- MELVILLE B.W. (1988), 'Scour at Bridges', Chapter 15 of Civil

- Engineering Practice 2 (Ed Cheremisinoff, P.N. Cheremisinoff, N.P., and Cheng, S.L), Technomic Publishing Co., Pennsylvania USA.
- NEILL, C.R. 1964, 'Local scour around bridge piers', Res, Council of Alberta, Highway and River Eng. Div.
- OLSEN, N.R.B. (1991). 'A three-Dimensional Numerical Model for Simulation of Sediment in Water Intake', *Dr. Ing. Dissertation*, The Norwegian Institute of Technology, Trondheim, Norway.
- OLSEN, N.R.B., MELAAEN, C.M. (1993). 'Three-Dimensional Calculation of Scour Around Cylinders', *J. Hydr. Engrg.* ASCE, Vol 119, No. 9, pp-1048-1054.
- PENSON, S. (1996) 'Investigation Of the Flow Around a pier Using the FLUENT package'. *M.Sc. (Eng) Thesis*, University of Liverpool.
- RAUDKIVI, A.J., 'Loose Boundary Hydraulics', 3rd Edition, Pergamon Press, 1990, pp. 142-210.
- RAUDKIVI, A.J. (1986). 'Functional Trends of Scour at Bridge Piers', *J. Hydr. Engrg.* ASCE, Vol 112, No1, pp.1-12.
- RAUDKIVI, A.J. and ETTEMA, R. (1977). 'Effect of Sediment Graduation on Clear Water Scour, Proceedings ASCE, Vol 103, No HY10, pp. 1209-1213.
- RIJN L. VAN, (1984). 'Sediment Transport' (in three parts). *H. Hydr. Engrg.* ASCE, Vol 110 (10, 11, 12).
- SHEN, H.W., SCHNEIDER, V.R. and KARAKI, S., 1969, 'Local scour around bridge piers', Proc, ASCE, 95, (HY6), pp 1919-1940.
- VANONI, V.A., (ed), (1975). 'Sedimentation Engineering', ASCE Manual No 54, New York: ASCE.
- YANMAZ, A.M., ALTINBILEK, H.D. (1991), 'Study of Time-Dependent Local Scour Around Bridge Piers', *J. Hydr. Engrg.* Vol 117, No.10, pp. 1247-1268.
- YANMAZ, A.M. (1994). - Personal Correspondence (1994).